ELSEVIER

Available online at www.sciencedirect.com

SCIENCE DIRECT®

International Journal of Solids and Structures 43 (2006) 4687–4703

INTERNATIONAL JOURNAL OF SOLIDS and STRUCTURES

www.elsevier.com/locate/ijsolstr

Optimization of tensegrity structures

Milenko Masic [a,*], Robert E. Skelton [a], Philip E. Gill [b]

[a] *Department of Mechanical and Aerospace Engineering, University of California San Diego, 9500 Gilman Drive, La Jolla, CA 92093-0411, United States*

[b] *Department of Mathematics, University of California San Diego, La Jolla, CA 92093-0112, United States*

Received 29 March 2005

Available online 5 October 2005

Abstract

This paper concerns the design of tensegrity structures with optimal mass-to-stiffness ratio. Starting from an initial layout that defines the largest set of allowed element connections, the procedure seeks the topology, geometry and prestress of the structure that yields optimal designs for different loading scenarios. The design constraints include strength constraints for all elements of the structure, buckling constraints for bars, and shape constraints. The problem formulation accommodates different symmetry constraints for structure parameters and shape. The static response of the structure is computed by using the nonlinear large displacement model. The problem is cast in the form of a nonlinear program. Examples show layouts of 2D and 3D asymmetric and symmetric structures. The influence of the material parameters on the optimal shape of the structure is investigated.

Keywords: Tensegrity; Optimization; Stiffness; Geometry

1. Introduction

A tensegrity structure is a prestressable truss-like system involving string elements capable of transmitting loads in one direction only. Admissible connections between elements are ball joints, and external loads can be applied only at the joints. Hence, all elements of the structure are axially loaded only, which greatly simplifies their static and dynamic modeling. This also enables the choice of materials and element geometry to be specialized for axial loads, and split further in materials optimized for compressive, and tensile stresses, and strains.

* Corresponding author. Tel.: +1 858 822 6679; fax: +1 858 822 3107.
E-mail address: mmasic@mae.ucsd.edu (M. Masic).

0020-7683/$ - see front matter
doi:10.1016/j.ijsolstr.2005.07.046

Recent increased interest in tensegrity structures is a result of their favorable properties. The extensive use of mechanically superior materials specialized for tensile loads allows the design of lightweight reconfigurable structures. Skelton and Adhikari (1998) recognized that tensegrity structures enable the integration of several functions within the same element. For example, string elements, that traditionally serve as load carrying members can also serve as actuators to control the structure as demonstrated by Masic and Skelton (2005). The current level of tensegrity technology development is characterized by the existence of successful dynamic models developed by Murakami (2001) and Skelton et al. (2001), and control strategies studied by Sultan et al. (2000, 2002), Masic and Skelton (2005) and Kanchanasaratool and Williamson (2002). A significant amount of research has been invested in tensegrity form-finding and rigidity analysis that can be characterized as static problems. This includes work of Pellegrino (1992), Motro (1992), Hanaor (1991), Connelly and Terrell (1995), Connelly and Whiteley (1996), Vasart and Motro (1999) and Masic et al. (2005).

As lightweight controllable structures are typically the target applications for tensegrities, there is a critical need for systematic methods for their optimal design. The contributions in this paper are motivated by the limitations of available methods. The optimization of the topology of structures has been studied for a long time (see, e.g., Save et al., 1985; Rozvany and Prager, 1989). Several approaches for numerical optimization have been proposed including those of Bendsoe and Kikuchi (1988), Diaz and Bendsoe (1992) and Bendsoe (1995), with recent approaches being free material modeling studied by Ben-Tal et al. (1999), and the optimization of trusses studied by Ben-Tal and Nemirovski (1997) and Jarre et al. (1998). In order to accommodate the specifics of tensegrity structures, our formulation of the problem includes tensegrity existence conditions that parameterize the prestressed equilibrium of the structure. Practical considerations require incorporating constraints that preserve structural integrity by preventing different modes of failure of its elements. In contrast to the optimization of trusses, analogous to that of Jarre et al. (1998), where the optimization starts from a fully populated grid, our formulation does not specify the maximum set of allowed geometries of the structure because nodal positions are actually design variables. This approach is essential for tensegrity optimization problems that must include a simultaneous search for a prestressble tensegrity form. We also consider the influence of different material parameters on the optimal topology.

The paper is organized as follows. In Section 2, we parameterize the equilibrium and static response of a structure and define the optimization variables and constraints. In Section 3, the problem is formulated as a nonlinear program and we derive the Jacobian of the nonlinear constraints. Several examples given in Section 4 are discussed in Section 5. We finish with some conclusions in Section 6.

2. Formulation of the problem

The objective of this analysis is the design tensegrity structures that have the maximum stiffness for a given mass of material. The total volume v_{total} can be used to fix the mass under the assumption that all elements are composed of the same material.

Let the set $\mathbb{N}$ of n_{n} nodes of a tensegrity structure be given, and let the position of each node $v_j \in \mathbb{N}$ be defined by the nodal vector $\mathbf{p}_j \in \mathbb{R}^3$. Let $\mathbb{P}$ denote the set of all nodal vectors. Assume that the set $\mathbb{E}$ of n_{e} elements of the structure are given, and let $\mathbb{E}_{\text{s}}$ and $\mathbb{E}_{\text{b}}$ denote the subsets of n_{s} strings and n_{b} bars respectively. We use the notation $e_i = \{[v_j, v_k], z_i\} \in \mathbb{E}$ to indicate that element e_i connects nodes v_j and v_k, where the scalar z_i identifies the type of the element, with

$$z_i = \begin{cases} 1 & \text{for } e_i \in \mathbb{E}_{\text{s}}, \\ -1 & \text{for } e_i \in \mathbb{E}_{\text{b}}. \end{cases} \tag{1}$$

2.1. Tensegrity equilibrium

If the element vector $\mathbf{g}_i \in \mathbb{R}^3$ associated with the element $e_i = \{[v_j, v_k], z_i\}$ is defined as

$$\mathbf{g}_i = \mathbf{p}_j - \mathbf{p}_k \quad \text{with } \|\mathbf{g}_i\|_2 = l_i,$$

then the element force vector $\mathbf{f}_{ji} \in \mathbb{R}^3$ representing the contribution of the internal force of the element e_i to the balance of the forces at the node v_j can be written as

$$\mathbf{f}_{ji} = c_{ji}\lambda_i \mathbf{g}_i \quad \text{with } f_i = \lambda_i \|\mathbf{g}_i\| = \lambda_i l_i, \tag{2}$$

where the element force density λ_i is a scalar. The scalars c_{ji} in (2) are typical elements of the matrix $C(\mathbb{E}) \in \mathbb{R}^{n_n \times n_e}$ and can take on one of the three possible values: $c_{ji} = \pm 1$ or $c_{ji} = 0$.

Let $\mathbb{R}^n_m$ denote the vector space of vectors $\mathbf{x}$ that have the following structure:

$$\mathbf{x} \in \mathbb{R}^n_m \Rightarrow \mathbf{x}^{\mathrm{T}} = \begin{bmatrix} \mathbf{x}_1^{\mathrm{T}} & \mathbf{x}_2^{\mathrm{T}} & \cdots & \mathbf{x}_n^{\mathrm{T}} \end{bmatrix}, \quad \mathbf{x}_i \in \mathbb{R}^m, \ \mathbb{R}^m = \mathbb{R}^m_1.$$

The vectors of nodal vectors $\mathbf{p} \in \mathbb{R}^{n_n}_3$, element vectors $\mathbf{g}(\mathbb{E}, \mathbf{p}) \in \mathbb{R}^{n_e}_3$, and force densities $\boldsymbol{\lambda} \in \mathbb{R}^{n_e}$, together with the vector $\mathbf{z} \in \mathbb{R}^{n_e}$ are formed by collecting the node vectors $\mathbf{p}_i$, element vectors $\mathbf{g}_i$, force densities λ_i, and individual element type identifiers, according to the definition

$$\mathbf{p}^{\mathrm{T}} = \begin{bmatrix} \mathbf{p}_1^{\mathrm{T}} & \cdots & \mathbf{p}_{n_n}^{\mathrm{T}} \end{bmatrix}, \quad \mathbf{g}^{\mathrm{T}} = \begin{bmatrix} \mathbf{g}_1^{\mathrm{T}} & \cdots & \mathbf{g}_{n_e}^{\mathrm{T}} \end{bmatrix}, \quad \boldsymbol{\lambda}^{\mathrm{T}} = \begin{bmatrix} \lambda_1 & \cdots & \lambda_{n_e} \end{bmatrix}, \quad \mathbf{z} = \begin{bmatrix} z_1 & \cdots & z_{n_e} \end{bmatrix}.$$

We define the linear operator $\tilde{(\cdot)}$ acting on the vector $\mathbf{x} \in \mathbb{R}^n_m$ as follows:

$$\tilde{\mathbf{x}} := \mathrm{blockdiag}(\mathbf{x}_1, \ldots, \mathbf{x}_i, \ldots, \mathbf{x}_n) \in \mathbb{R}^{mn \times n}, \quad \mathbf{x}_i \in \mathbb{R}^m.$$

Similarly, the linear operator $\hat{(\cdot)}$ acting on the vector $\mathbf{x} \in \mathbb{R}^n$ is given by

$$\hat{\mathbf{x}} := \tilde{\mathbf{x}} \otimes I_3 \in \mathbb{R}^{3n \times 3n}.$$

Let the member-node incidence matrix of the oriented graph associated with $\mathbb{E}$ be denoted by $M(\mathbb{E}) \in \mathbb{R}^{n_e \times n_n}$, and let $\mathbf{M} \in \mathbb{R}^{3n_e \times 3n_n}$ be defined as $\mathbf{M} = M \otimes I_3$. A typical element m_{ij} of the matrix M is $m_{ij} = 1$ if the element e_i terminates at the node v_j, and $m_{ij} = -1$ if the element e_i emanates from the node v_j. Otherwise $m_{ij} = 0$. If we assume that the n_s string elements in $\mathbb{E}_s$ appear first, then the vector $\mathbf{g}$ and matrix $\mathbf{M}$ are related and partitioned as follows:

$$\mathbf{g}(\mathbf{p}) = \begin{bmatrix} \mathbf{g}_s(\mathbf{p}) \\ \mathbf{g}_b(\mathbf{p}) \end{bmatrix} = \mathbf{M}\mathbf{p}, \qquad \mathbf{M} = \begin{bmatrix} \mathbf{S}^{\mathrm{T}} \\ \mathbf{B}^{\mathrm{T}} \end{bmatrix}, \quad \mathbf{S} \in \mathbf{R}^{3n_n \times 3n_s}.$$

Similarly, it can be shown that the matrices $\mathbf{M}(\mathbb{E})$ and $\mathbf{C}(\mathbb{E}) = C(\mathbb{E}) \otimes I_3$ are related as follows:

$$\mathbf{M} = \begin{bmatrix} \mathbf{S}^{\mathrm{T}} \\ \mathbf{B}^{\mathrm{T}} \end{bmatrix}, \qquad \mathbf{C} = \begin{bmatrix} -\mathbf{S} & \mathbf{B} \end{bmatrix}.$$

Throughout, it will be assumed that the string elements of the tensegrity structure are numbered first, so that the vectors $(\cdot) \in \mathbb{R}^{n_e}_m$ of all different properties associated with the elements of the structure can be partitioned so that

$$(\cdot) = \begin{bmatrix} (\cdot)_s \\ (\cdot)_b \end{bmatrix}, \quad (\cdot)_s \in \mathbb{R}^{n_s}_m, \ (\cdot)_b \in \mathbb{R}^{n_b}_m.$$

For a given configuration $\mathbf{p}$, let $\mathbf{f}^e_j(\mathbf{p}) \in \mathbb{R}^3$ and $\mathbf{f}^c_j(\mathbf{p}) \in \mathbb{R}^3$ represent the respective collection of external force vectors and constraint forces acting at the node v_j, i.e.,

$$\mathbf{f}^{e\,\mathrm{T}} = \begin{bmatrix} \mathbf{f}_1^{e\,\mathrm{T}} & \mathbf{f}_2^{e\,\mathrm{T}} & \cdots & \mathbf{f}_{n_n}^{e\,\mathrm{T}} \end{bmatrix}, \qquad \mathbf{f}^{c\,\mathrm{T}} = \begin{bmatrix} \mathbf{f}_1^{c\,\mathrm{T}} & \mathbf{f}_2^{c\,\mathrm{T}} & \cdots & \mathbf{f}_{n_n}^{c\,\mathrm{T}} \end{bmatrix}.$$

It follows that the equilibrium conditions for the structure with properly loaded strings in the configuration $\mathbf{p}$ can be written as:

$$\mathbf{C}\hat{\boldsymbol{\lambda}}(\mathbf{p})\mathbf{M}\mathbf{p} + \mathbf{f}^{\mathrm{e}}(\mathbf{p}) + \mathbf{f}^{\mathrm{c}}(\mathbf{p}) = 0, \tag{3}$$

$$\lambda_i(\mathbf{p}) \geqslant 0, \quad e_i \in \mathbb{E}_{\mathrm{s}}. \tag{4}$$

2.1.1. The constitutive equations

The relationship between the force–density variables $\boldsymbol{\lambda}(\mathbf{p})$ and the actual structure parameters depends on the strain–stress relationship for the material used to build the elastic elements of the structure. The force densities $\boldsymbol{\lambda}(\mathbf{p})$ at any equilibrium configuration $\mathbf{p}$ can be computed from Hooke's law for linear elastic materials. We define the volumes v_i, rest lengths l_{0_i} and Young's modulus y_i of cylindrical elements and form the corresponding vectors $\mathbf{l}_0 \in \mathbb{R}^{n_{\mathrm{e}}}$, $\mathbf{v} \in \mathbb{R}^{n_{\mathrm{e}}}$ and $\mathbf{y} \in \mathbb{R}^{n_{\mathrm{e}}}$, such that

$$\mathbf{l}_0 = \begin{bmatrix} l_{0_1} \\ l_{0_2} \\ \vdots \\ l_{0_{n_{\mathrm{e}}}} \end{bmatrix} = \begin{bmatrix} \mathbf{l}_{0_{\mathrm{s}}} \\ \mathbf{l}_{0_{\mathrm{b}}} \end{bmatrix}, \quad \mathbf{v} = \begin{bmatrix} v_1 \\ v_2 \\ \vdots \\ v_{n_{\mathrm{e}}} \end{bmatrix} = \begin{bmatrix} \mathbf{v}_{\mathrm{s}} \\ \mathbf{v}_{\mathrm{b}} \end{bmatrix}, \quad \mathbf{y} = \begin{bmatrix} y_1 \\ y_2 \\ \vdots \\ y_{n_{\mathrm{n}}} \end{bmatrix} = \begin{bmatrix} \mathbf{y}_{\mathrm{s}} \\ \mathbf{y}_{\mathrm{b}} \end{bmatrix}.$$

Then the force densities can be computed as

$$\lambda_i(\mathbf{p}) = \frac{\mathbf{f}_i(\mathbf{p})}{l_i(\mathbf{p})} = z_i \frac{y_i v_i}{l_i(\mathbf{p}) l_{0_i}^2}(l_i(\mathbf{p}) - l_{0_i}). \tag{5}$$

Note that constraint (4) is then equivalent to

$$-(l_i(\mathbf{p}) - l_{0_i}) \leqslant 0, \quad e_i \in \mathbb{E}_{\mathrm{s}}. \tag{6}$$

2.1.2. Equilibrium conditions in the absence of external forces

If there is no external load, then $\mathbf{f}^{\mathrm{e}}(\mathbf{p}) = 0$ and the equilibrium condition in (3) becomes

$$\mathbf{C}\hat{\boldsymbol{\lambda}}(\mathbf{p})\mathbf{M}\mathbf{p} + \mathbf{f}^{\mathrm{c}}(\mathbf{p}) = 0, \tag{7}$$

$$-(l_i(\mathbf{p}) - l_{0_i}) \leqslant 0, \quad e_i \in \mathbb{E}_{\mathrm{s}}, \tag{8}$$

where $\boldsymbol{\lambda}(\mathbf{p})$ is given by (5).

2.2. Large displacement static response—the loaded equilibrium conditions

Once the external force $\mathbf{f}^{\mathrm{e}}$ is applied to the structure in an equilibrium configuration $\mathbf{p}$, it deforms to a new equilibrium configuration, $\mathbf{p} + \mathbf{u}$. The vector of nodal displacements $\mathbf{u} \in \mathbb{R}_3^{n_{\mathrm{n}}}$ such that

$$\mathbf{u}^{\mathrm{T}} = \begin{bmatrix} \mathbf{u}_1^{\mathrm{T}} & \mathbf{u}_2^{\mathrm{T}} & \cdots & \mathbf{u}_{n_{\mathrm{n}}}^{\mathrm{T}} \end{bmatrix}$$

can be computed without any assumptions on the size of the displacement $\mathbf{u}_j \in \mathbb{R}^3$ of the node v_j. Eq. (5) defines the equilibrium force coefficient vector $\boldsymbol{\lambda}(\mathbf{p} + \mathbf{u})$ in any equilibrium configuration $\mathbf{p} + \mathbf{u}$, and this relationship holds regardless of the magnitude of $\mathbf{u}$. It follows that nodal displacements $\mathbf{u}$ of the loaded structure can be computed directly from the structure equilibrium conditions in the configuration $\mathbf{p} + \mathbf{u}$ instead of being defined using a linearization method involving the structure stiffness matrix. From (3), substituting (4) with (6), equilibrium conditions for the configuration $\mathbf{p} + \mathbf{u}$ become

$$\mathbf{C}\hat{\boldsymbol{\lambda}}(\mathbf{p}+\mathbf{u})\mathbf{M}(\mathbf{p}+\mathbf{u}) + \mathbf{f}^{\mathrm{e}}(\mathbf{p}+\mathbf{u}) + \mathbf{f}^{\mathrm{c}}(\mathbf{p}+\mathbf{u}) = 0, \tag{9}$$

$$-\left(l_i(\mathbf{p}+\mathbf{u}) - l_{0_i}\right) \leqslant 0, \quad e_i \in \mathbb{E}_{\mathrm{s}}, \tag{10}$$

where $\boldsymbol{\lambda}(\mathbf{p}+\mathbf{u})$ is given by (5). The constraint in (10) guarantees that the string elements are not compressed in the new equilibrium.

The relationship between the nodal displacements $\mathbf{u}$ and the external forces $\mathbf{f}^{\mathrm{e}}$ in (9) is nonlinear, although the elements of the structure are linear elastic. The nonlinear structure model in (9) parameterizes all equilibrium configurations of the structure under the external force $\mathbf{f}^{\mathrm{e}}$, regardless of whether or not the configuration is unique. It can be seen that the non-uniqueness of the equilibrium geometry $\mathbf{p}+\mathbf{u}$ resulting from global buckling or other nonlinear effects is also accommodated by this model.

2.3. Defining the optimization objective and identifying design variables

2.3.1. The objective function

Different criteria can be defined to measure the structure stiffness. One possible measure is the work done by the external forces $\mathbf{f}^{\mathrm{e}}$ in deforming the structure from configuration $\mathbf{p}$ to $\mathbf{p}+\mathbf{u}$. The inner product, $\frac{1}{2}\mathbf{f}^{\mathrm{e}\,\mathrm{T}}\mathbf{u}$, is an approximation of the deformation work and will be called the *approximate compliance* since it is computed from the nonlinear structure model (9). Computed values of the approximate compliance, $\frac{1}{2}\mathbf{f}^{\mathrm{e}\,\mathrm{T}}\mathbf{u}$, are generally lower than the compliance $\frac{1}{2}\mathbf{f}^{\mathrm{e}\,\mathrm{T}}\mathbf{u}^{\mathrm{l}}$, if the nodal displacements, $\mathbf{u}^{\mathrm{l}}$, are computed from the linearized structure model. This is because of the nonlinear stiffening effect.

If the approximate compliance is used as the measure of the stiffness, only the nodal displacements of the nodes at which the external forces act are penalized. An elliptical norm $\mathbf{u}^{\mathrm{T}}Q\mathbf{u}$ with $Q \succeq 0$ can be used as the stiffness measure to penalize other nodal displacements.

2.3.2. The design variables

For a tensegrity structure with connectivity $\mathbb{E}$, it is clear from (3), (4), (9), (10) and (5) that the parameters that define its static response $\mathbf{u}$ are the nodal vector $\mathbf{p}$, element rest lengths $\mathbf{l}_0 \in \mathbb{R}^{n_{\mathrm{e}}}$, and element volumes $\mathbf{v} \in \mathbb{R}^{n_{\mathrm{e}}}$. These three structure parameters are variables in the optimization problem. The domains of their feasible values are $\mathbf{l}_0 > 0$ and $\mathbf{v} \geqslant 0$. Note that although the presence of the element e_i in the set $\mathbb{E}$ defines the allowable element connections in the structure, it is value of the volume $v_i > 0$ that actually defines whether or not an element is present. For a structure consisting of elements built of the same material, the constraint that fixes the total mass is written as $\sum v_i = v_{\mathrm{total}}$.

2.3.3. The treatment of symmetry

For efficiency, the number of problem variables must be reduced to account for any symmetry in the design. With the structure parameters identified so far, there are two classes of symmetry. The first symmetry is the nodal symmetry. It can be shown that the nodal symmetry constraint can be cast in the following linear form:

$$\mathbf{p} = \mathscr{R}\underline{\mathbf{p}},$$

where the matrix $\mathscr{R}$ depends on the particular type of nodal symmetry and is defined in Masic et al. (2005). Obviously, the nodal symmetry constraint represents a reduction in the number of independent geometry variables from $\mathbf{p} \in \mathbb{R}^{n_{\mathrm{n}}}_3$ to $\underline{\mathbf{p}} \in \mathbb{R}^{n_{\mathrm{c}}}_3$, where the vector $\underline{\mathbf{p}}$ is the nodal vector of the subset of nodes $\underline{\mathbb{N}} \in \mathbb{N}$. The second symmetry is the symmetry of the sets of parameters $\mathbf{l}_0$ and $\mathbf{v}$ associated with the elements of the structure. It can also be regarded as a reduction of the number of variables and cast in the linear form

$$\mathbf{l}_0 = E\underline{\mathbf{l}}_0, \quad \mathbf{v} = E\underline{\mathbf{v}}, \quad E \in \mathbb{R}^{n_{\mathrm{e}} \times \underline{n}_{\mathrm{e}}}, \qquad \underline{\mathbf{l}}_0, \underline{\mathbf{v}} \in \mathbb{R}^{\underline{n}_{\mathrm{e}}},$$

where the sparse matrix E relates the vector of different typical elements with the full vector of the variables. It is possible to define other symmetries of the structure. Symmetry of the external force and nodal displacements are two such examples. These additional symmetries will not be exploited in the problem formulation because they are not independent of each other, and if they are not defined consistently they can define constraints with no feasible point.

2.4. Shape constraints and boundary conditions

2.4.1. Shape constraints

A desired shape of the structure can be specified before external forces $\mathbf{f}^{\mathrm{e}}$ are applied to it by defining a general shape constraint of the form $\boldsymbol{\varphi}(\underline{\mathbf{p}}) = 0$. To ensure that the tensegrity structure can be supported at the desired locations and that the external load can be attached to it at specified locations, the tensegrity structure in the configuration $\mathbf{p} = \mathscr{R}\underline{\mathbf{p}}$ must satisfy the shape constraints in the linear form,

$$\mathbf{P}\underline{\mathbf{p}} = \underline{\mathbf{p}}^{\mathrm{c}},$$

where $\mathbf{P}$ and $\underline{\mathbf{p}}^{\mathrm{c}}$ are a given matrix and vector.

There are also geometry constraints involving a restriction on the minimum length of an element, i.e.,

$$l_i(\mathbf{p}) > l_{\min_i}, \qquad l_i(\mathbf{p}+\mathbf{u}) > l_{\min_i}.$$

One reason for this constraint is the difficulty of manufacturing structures with elements that are too short. As the elements of the constraint Jacobian involve the inverse of the element lengths, this constraint also serves to guarantee that the constraint Jacobian is well defined.

2.4.2. Treatment of the boundary conditions

The only constraint on the structure displacements $\mathbf{u}$ that will be considered here is the consequence of attaching the nodes of the structure to linear supports. In this case the admissible nodal displacements must satisfy the linear constraint

$$C_u\mathbf{u} = 0,$$

where the structure of the constraint matrix $C_u \in \mathbb{R}^{n_{\mathrm{c}}\times 3n_{\mathrm{n}}}$ depends on the type of supports that the structure is attached to. It can be shown that the constraint forces, $\mathbf{f}^{\mathrm{c}}(\mathbf{p})$, in any configuration $\mathbf{p}$, are the vectors in the left range space of the matrix C_u. Hence, $\mathbf{f}^{\mathrm{c}}(\mathbf{p})$ can be written as

$$\mathbf{f}^{\mathrm{c}}(\mathbf{p}) = C_u^{\mathrm{T}}\boldsymbol{\lambda}^{\mathrm{c}}(\mathbf{p}) \tag{11}$$

for some choice of Lagrange multipliers $\boldsymbol{\lambda}^{\mathrm{c}} \in \mathbb{R}^{n_{\mathrm{c}}}$. Assume that only n_{c} independent boundary conditions are defined, in which case the matrix C_u has full row rank. Let the singular-value decomposition of C_u be written as

$$C_u = U\Sigma V^{\mathrm{T}} = U[\,\Sigma_1 \quad 0\,]\begin{bmatrix} V_1^{\mathrm{T}} \\ V_2^{\mathrm{T}} \end{bmatrix} = U\Sigma_1 V_1^{\mathrm{T}}, \qquad C_u^{\mathrm{T}} = V_1\Sigma_1 U^{\mathrm{T}},$$

$$UU^{\mathrm{T}} = U^{\mathrm{T}}U = I, \qquad VV^{\mathrm{T}} = V^{\mathrm{T}}V = I.$$

An equivalent formulation of the equilibrium conditions (9) and (3) can be derived by using (11) in these equations and multiplying them from the left with the orthonormal full rank matrix V^{T}. This gives

$$\begin{bmatrix} V_1^{\mathrm{T}} \\ V_2^{\mathrm{T}} \end{bmatrix}(\mathbf{C}\hat{\boldsymbol{\lambda}}(\mathbf{p})\mathbf{M}(\mathbf{p}) + \mathbf{f}^{\mathrm{e}}(\mathbf{p})) + \begin{bmatrix} \Sigma_1 U^{\mathrm{T}} \\ 0 \end{bmatrix}\boldsymbol{\lambda}^{\mathrm{c}}(\mathbf{p}) = 0. \tag{12}$$

It is clear from (12) that the solution can be split into two parts. The Lagrange multipliers $\boldsymbol{\lambda}^{\mathrm{c}}$ do not appear in the first set of equations

$$V_2^{\mathrm{T}}(\mathbf{C}\hat{\boldsymbol{\lambda}}(\mathbf{p})\mathbf{M}(\mathbf{p}) + \mathbf{f}^{\mathrm{e}}(\mathbf{p})) = 0,$$

whereas the second set of equations

$$V_1^{\mathrm{T}}(\mathbf{C}\hat{\boldsymbol{\lambda}}(\mathbf{p})\mathbf{M}(\mathbf{p}) + \mathbf{f}^{\mathrm{e}}(\mathbf{p})) + \Sigma_1 U^{\mathrm{T}}\boldsymbol{\lambda}^{\mathrm{c}}(\mathbf{p}) = 0$$

can be solved directly for the Lagrange multipliers $\boldsymbol{\lambda}^{\mathrm{c}}$ and the constraint forces $\mathbf{f}^{\mathrm{c}}$, i.e.,

$$\boldsymbol{\lambda}^{\mathrm{c}}(\mathbf{p}) = -U\Sigma_1^{-1}V_1^{\mathrm{T}}(\mathbf{C}\hat{\boldsymbol{\lambda}}(\mathbf{p})\mathbf{M}(\mathbf{p}) + \mathbf{f}^{\mathrm{e}}(\mathbf{p})),$$
$$\mathbf{f}^{\mathrm{c}}(\mathbf{p}) = C_u^{\mathrm{T}}\boldsymbol{\lambda}^{\mathrm{c}}(\mathbf{p}) = -C_u^{\mathrm{T}}U\Sigma_1^{-1}V_1^{\mathrm{T}}(\mathbf{C}\hat{\boldsymbol{\lambda}}(\mathbf{p})\mathbf{M}(\mathbf{p}) + \mathbf{f}^{\mathrm{e}}(\mathbf{p})).$$

2.5. Strength constraints

All elements of a tensegrity structure must be prevented from yielding in order to preserve structure integrity in both the unloaded configuration $\mathbf{p}$ and the loaded configuration $\mathbf{p} + \mathbf{u}$. Constraints that prevent yielding can be defined by applying Hooke's law to the axially loaded elements, i.e.,

$$\epsilon_i(\mathbf{p})y_i = z_i\frac{l_i(\mathbf{p}) - l_{0_i}}{l_{0_i}}y_i \leqslant \sigma_i,$$
$$\epsilon_i(\mathbf{p}+\mathbf{u})y_i = z_i\frac{l_i(\mathbf{p}+\mathbf{u}) - l_{0_i}}{l_{0_i}}y_i \leqslant \sigma_i,$$

where σ_i is the yield stress of the element e_i. An equivalent form of these constraints is

$$z_i(l_i(\mathbf{p}) - l_{0_i})y_i - \sigma_i l_{0_i} \leqslant 0,$$
$$z_i(l_i(\mathbf{p}+\mathbf{u}) - l_{0_i})y_i - \sigma_i l_{0_i} \leqslant 0.$$

Additional constraints account for the fact that bar elements are allowed to be under tension

$$y_i(l_i(\mathbf{p}) - l_{0_i}) - l_{0_i}\sigma \leqslant 0, \quad e_i \in \mathbb{E}_{\mathrm{b}},$$
$$y_i(l_i(\mathbf{p}+\mathbf{u}) - l_{0_i}) - l_{0_i}\sigma \leqslant 0, \quad e_i \in \mathbb{E}_{\mathrm{b}}.$$

2.6. Buckling constraints

Buckling constraints are applied to bars only because bar elements are the only elements that may be compressed. The maximum magnitude, $f_{\max_i}$, of the compressive force, f_i, that the bars can be loaded with, is defined by Euler's formula

$$f_i \leqslant f_{\max_i} = \frac{\pi^2 y_i I_{\min_i}}{l_{0_i}^2}, \tag{13}$$

where $I_{\min_i}$ is the minimal moment of inertia of the cross section of the element. Assuming that all bars have a round cross section with radius r_i, the quantity $I_{\min_i}$ is defined as

$$I_{\min_i} = \frac{\pi r_i^4}{4}.$$

Then, using

$$r_i^2 = \frac{v_i}{\pi l_{0_i}},$$

the quantity $I_{\min_i}$ can be computed as

$$I_{\min_i} = \frac{v_i^2}{4\pi l_{0_i}^2}. \tag{14}$$

From (2), (5) and (14) after manipulating (13), the bar buckling constraint can be rewritten as

$$-l_0^2(l_i(\mathbf{p}) - l_{0_i}) - \frac{\pi}{4} v_i \leqslant 0, \quad e_i \in \mathbb{E}_\mathrm{b}.$$

The buckling constraint must be satisfied in both the unloaded configuration $\mathbf{p}$ and the loaded configuration $\mathbf{p}+\mathbf{u}$. It follows that:

$$-l_0^2(l_i(\mathbf{p}) - l_{0_i}) - \frac{\pi}{4} v_i \leqslant 0, \quad e_i \in \mathbb{E}_\mathrm{b},$$
$$-l_0^2(l_i(\mathbf{p}+\mathbf{u}) - l_{0_i}) - \frac{\pi}{4} v_i \leqslant 0, \quad e_i \in \mathbb{E}_\mathrm{b}.$$

3. Nonlinear program formulation

Enforcing strength and buckling constraints for zero volume elements may produce conservative results. Hence, these constraints should be relaxed by multiplying them by the element volume v_i. The optimal mass-to-stiffness ratio optimization problem for the tensegrity structure of the connectivity $\mathbb{E}$, made of the material $\{y, \sigma\}$, loaded with external force $\mathbf{f}^\mathrm{e}$, and defined shape and displacement constraints is written as

Given data
$\mathbf{C}(\mathbb{E}), \mathbf{M}(\mathbb{E}), \mathbf{z}, \mathbf{y}, \mathbf{f}^\mathrm{e}, \mathbf{C}_u, V_2, \mathbf{P}, \underline{\mathbf{p}}^\mathrm{c}, \mathscr{R}, E, \sigma, v_\mathrm{total}, \mathbf{l}_{0\min}, \mathbf{l}_\mathrm{min}, \bar{\mathbf{l}}_\mathrm{min},$

$\min_{\underline{\mathbf{p}}, \underline{\mathbf{l}}_0, \underline{\mathbf{v}}, \mathbf{u}}$ $\mathbf{f}^{\mathrm{e}\,\mathrm{T}}\mathbf{u}$,

subject to

linear constraints:
$\mathbf{P}\underline{\mathbf{p}} = \underline{\mathbf{p}}^\mathrm{c}$,
$-\underline{\mathbf{l}}_0 + \mathbf{l}_{0\min} \leqslant 0$,
$-\underline{\mathbf{v}} \leqslant 0$,
$[1 \quad 1 \quad \cdots \quad 1]\mathbf{v} - v_\mathrm{total} = 0$,
$\mathbf{C}_u\mathbf{u} = 0$,

nonlinear constraints:
$\boldsymbol{\varphi}(\underline{\mathbf{p}}) = 0$,
$V_2^\mathrm{T}\mathbf{C}\hat{\boldsymbol{\lambda}}(\mathbf{p})\mathbf{M}\mathbf{p} = 0$,
$V_2^\mathrm{T}\mathbf{C}\hat{\boldsymbol{\lambda}}(\mathbf{p}+\mathbf{u})\mathbf{M}(\mathbf{p}+\mathbf{u}) + V_2^\mathrm{T}\mathbf{f}^\mathrm{e} = 0$,
$-\tilde{\mathbf{v}}_\mathrm{s}(\mathbf{l}_\mathrm{s}(\mathbf{p}) - \mathbf{l}_{0_\mathrm{s}}) \leqslant 0$,
$-\tilde{\mathbf{v}}_\mathrm{s}(\mathbf{l}_\mathrm{s}(\mathbf{p}+\mathbf{u}) - \mathbf{l}_{0_\mathrm{s}}) \leqslant 0$,
$-\mathbf{l}(\mathbf{p}) + \mathbf{l}_\mathrm{min} \leqslant 0$,
$-\mathbf{l}(\mathbf{p}+\mathbf{u}) + \bar{\mathbf{l}}_\mathrm{min} \leqslant 0$,
$\tilde{\mathbf{v}}(\tilde{\mathbf{z}}\tilde{\mathbf{y}}(\mathbf{l}(\mathbf{p}) - \mathbf{l}_0) - \tilde{\boldsymbol{\sigma}}\mathbf{l}_0) \leqslant 0$,
$\tilde{\mathbf{v}}_\mathrm{b}(\tilde{\mathbf{y}}_\mathrm{b}(\mathbf{l}_\mathrm{b}(\mathbf{p}) - \mathbf{l}_{0_\mathrm{b}}) - \tilde{\boldsymbol{\sigma}}_\mathrm{b}\mathbf{l}_{0_\mathrm{b}}) \leqslant 0$,
$\tilde{\mathbf{v}}(\tilde{\mathbf{z}}\tilde{\mathbf{y}}(\mathbf{l}(\mathbf{p}+\mathbf{u}) - \mathbf{l}_0) - \tilde{\boldsymbol{\sigma}}\mathbf{l}_0) \leqslant 0$,
$\tilde{\mathbf{v}}_\mathrm{b}(\tilde{\mathbf{y}}_\mathrm{b}(\mathbf{l}_\mathrm{b}(\mathbf{p}+\mathbf{u}) - \mathbf{l}_{0_\mathrm{b}}) - \tilde{\boldsymbol{\sigma}}_\mathrm{b}\mathbf{l}_{0_\mathrm{b}}) \leqslant 0$,
$-\tilde{\mathbf{v}}_\mathrm{b}(\tilde{\mathbf{l}}_{0_\mathrm{b}}^2(\mathbf{l}_\mathrm{b}(\mathbf{p}) - \mathbf{l}_{0_\mathrm{b}}) - \frac{\pi}{4}\mathbf{v}_\mathrm{b}) \leqslant 0$,
$-\tilde{\mathbf{v}}_\mathrm{b}(\tilde{\mathbf{l}}_{0_\mathrm{b}}^2(\mathbf{l}_\mathrm{b}(\mathbf{p}+\mathbf{u}) - \mathbf{l}_{0_\mathrm{b}}) - \frac{\pi}{4}\mathbf{v}_\mathrm{b}) \leqslant 0$,

where $\mathbf{p} = \mathscr{R}\underline{\mathbf{p}}, \quad l_i(\mathbf{p}) = \|\mathbf{g}_i(\mathbf{p})\|_2, \quad \mathbf{g}(\mathbf{p}) = \mathbf{M}\mathbf{p},$

$$\mathbf{l}_0 = E\underline{\mathbf{l}}_0, \quad \mathbf{v} = E\underline{\mathbf{y}},$$

$$\lambda_i(\mathbf{p}) = \frac{z_i y_i v_i}{l_i(\mathbf{p}) l_{0_i}^2}(l_i(\mathbf{p}) - l_{0_i}).$$

3.1. Jacobian of the nonlinear constraints

The Jacobian of the nonlinear constraints is given in the following matrix, where $\bar{x}$ denotes $\bar{x} = x(\mathbf{p} + \mathbf{u})$:

$$J = \begin{bmatrix}
\delta\boldsymbol{\varphi}(\underline{\mathbf{p}})/\delta\underline{\mathbf{p}} & 0 & 0 & 0 \\
V_2^{\mathrm{T}}\mathbf{C}\hat{\boldsymbol{\lambda}}\mathbf{M} - V_2^{\mathrm{T}}\mathbf{C}\tilde{\mathbf{g}}\tilde{\mathbf{y}}\tilde{\mathbf{v}}\tilde{\mathbf{l}}_0^{-1}\tilde{\mathbf{l}}^{-3}\tilde{\mathbf{g}}^{\mathrm{T}}\mathbf{C}^{\mathrm{T}} & V_2^{\mathrm{T}}\mathbf{C}\tilde{\mathbf{g}}\tilde{\mathbf{z}}\tilde{\mathbf{y}}\tilde{\mathbf{v}}(-2\tilde{\mathbf{l}}_0^{-3} + \tilde{\mathbf{l}}_0^{-2}\tilde{\mathbf{l}}^{-1}) & V_2^{\mathrm{T}}\mathbf{C}\tilde{\mathbf{g}}\tilde{\mathbf{z}}\tilde{\mathbf{y}}\tilde{\mathbf{l}}_0^{-2}\tilde{\mathbf{l}}^{-1}(\tilde{\mathbf{l}} - \tilde{\mathbf{l}}_0) & 0 \\
V_2^{\mathrm{T}}\mathbf{C}\hat{\boldsymbol{\lambda}}\mathbf{M} - V_2^{\mathrm{T}}C\tilde{\mathbf{g}}\tilde{\mathbf{y}}\tilde{\mathbf{v}}\tilde{\mathbf{l}}_0^{-1}\tilde{\tilde{\mathbf{l}}}^{-3}\tilde{\tilde{\mathbf{g}}}^{\mathrm{T}}\mathbf{C}^{\mathrm{T}} & V_2^{\mathrm{T}}\mathbf{C}\tilde{\mathbf{g}}\tilde{\mathbf{z}}\tilde{\mathbf{y}}\tilde{\mathbf{v}}(-2\tilde{\mathbf{l}}_0^{-3} + \tilde{\mathbf{l}}_0^{-2}\tilde{\tilde{\mathbf{l}}}^{-1}) & V_2^{\mathrm{T}}\mathbf{C}\tilde{\mathbf{g}}\tilde{\mathbf{z}}\tilde{\mathbf{y}}\tilde{\mathbf{l}}_0^{-2}\tilde{\tilde{\mathbf{l}}}^{-1}(\tilde{\tilde{\mathbf{l}}} - \tilde{\mathbf{l}}_0) & V_2^{\mathrm{T}}\mathbf{C}\hat{\boldsymbol{\lambda}}\mathbf{M} - V_2^{\mathrm{T}}C\tilde{\mathbf{g}}\tilde{\mathbf{y}}\tilde{\mathbf{v}}\tilde{\mathbf{l}}_0^{-1}\tilde{\tilde{\mathbf{l}}}^{-3}\tilde{\tilde{\mathbf{g}}}^{\mathrm{T}}\mathbf{C}^{\mathrm{T}} \\
\tilde{\mathbf{v}}_{\mathrm{s}}\tilde{\mathbf{l}}_{\mathrm{s}}^{-1}\tilde{\mathbf{g}}_{\mathrm{s}}^{\mathrm{T}}\mathbf{S}^{\mathrm{T}} & \tilde{\mathbf{v}}_{\mathrm{s}} & -(\tilde{\mathbf{l}}_{\mathrm{s}} - \tilde{\mathbf{l}}_{0_{\mathrm{s}}}) & 0 \\
\tilde{\mathbf{v}}_{\mathrm{s}}\tilde{\tilde{\mathbf{l}}}_{\mathrm{s}}^{-1}\tilde{\tilde{\mathbf{g}}}_{\mathrm{s}}^{\mathrm{T}}\mathbf{S}^{\mathrm{T}} & \tilde{\mathbf{v}}_{\mathrm{s}} & -(\tilde{\tilde{\mathbf{l}}}_{\mathrm{s}} - \tilde{\mathbf{l}}_{0_{\mathrm{s}}}) & \tilde{\mathbf{v}}_{\mathrm{s}}\tilde{\tilde{\mathbf{l}}}_{\mathrm{s}}^{-1}\tilde{\tilde{\mathbf{g}}}_{\mathrm{s}}^{\mathrm{T}}\mathbf{S}^{\mathrm{T}} \\
-\tilde{\mathbf{l}}^{-1}\tilde{\mathbf{g}}^{\mathrm{T}}\mathbf{M} & 0 & 0 & 0 \\
-\tilde{\tilde{\mathbf{l}}}^{-1}\tilde{\tilde{\mathbf{g}}}^{\mathrm{T}}\mathbf{M} & 0 & 0 & -\tilde{\tilde{\mathbf{l}}}^{-1}\tilde{\tilde{\mathbf{g}}}^{\mathrm{T}}\mathbf{M} \\
\tilde{\mathbf{z}}\tilde{\mathbf{v}}\tilde{\mathbf{y}}\tilde{\mathbf{l}}^{-1}\tilde{\mathbf{g}}^{\mathrm{T}}\mathbf{M} & -\tilde{\mathbf{z}}\tilde{\mathbf{y}}\tilde{\mathbf{v}} - \tilde{\boldsymbol{\sigma}}\tilde{\mathbf{v}} & \tilde{\mathbf{z}}\tilde{\mathbf{y}}(\tilde{\mathbf{l}} - \tilde{\mathbf{l}}_0) - \tilde{\mathbf{l}}_0\tilde{\boldsymbol{\sigma}} & 0 \\
\tilde{\mathbf{v}}_{\mathrm{b}}\tilde{\mathbf{y}}_{\mathrm{b}}\tilde{\mathbf{l}}_{\mathrm{b}}^{-1}\tilde{\mathbf{g}}_{\mathrm{b}}^{\mathrm{T}}\mathbf{B}^{\mathrm{T}} & \tilde{\mathbf{y}}_{\mathrm{b}}\tilde{\mathbf{v}}_{\mathrm{b}} - \tilde{\boldsymbol{\sigma}}_{\mathrm{b}}\tilde{\mathbf{v}}_{\mathrm{b}} & \tilde{\mathbf{y}}_{\mathrm{b}}(\tilde{\mathbf{l}}_{\mathrm{b}} - \tilde{\mathbf{l}}_{0_{\mathrm{b}}}) - \tilde{\mathbf{l}}_{0_{\mathrm{b}}}\tilde{\boldsymbol{\sigma}}_{\mathrm{b}} & 0 \\
\tilde{\mathbf{z}}\tilde{\mathbf{v}}\tilde{\mathbf{y}}\tilde{\tilde{\mathbf{l}}}^{-1}\tilde{\tilde{\mathbf{g}}}^{\mathrm{T}}\mathbf{M} & -\tilde{\mathbf{z}}\tilde{\mathbf{y}}\tilde{\mathbf{v}} - \tilde{\boldsymbol{\sigma}}\tilde{\mathbf{v}} & \tilde{\mathbf{z}}\tilde{\mathbf{y}}(\tilde{\tilde{\mathbf{l}}} - \tilde{\mathbf{l}}_0) - \tilde{\mathbf{l}}_0\tilde{\boldsymbol{\sigma}} & \tilde{\mathbf{z}}\tilde{\mathbf{v}}\tilde{\mathbf{y}}\tilde{\tilde{\mathbf{l}}}^{-1}\tilde{\tilde{\mathbf{g}}}^{\mathrm{T}}\mathbf{M} \\
\tilde{\mathbf{v}}_{\mathrm{b}}\tilde{\mathbf{y}}_{\mathrm{b}}\tilde{\tilde{\mathbf{l}}}_{\mathrm{b}}^{-1}\tilde{\tilde{\mathbf{g}}}_{\mathrm{b}}^{\mathrm{T}}\mathbf{B}^{\mathrm{T}} & \tilde{\mathbf{y}}_{\mathrm{b}}\tilde{\mathbf{v}}_{\mathrm{b}} - \tilde{\boldsymbol{\sigma}}_{\mathrm{b}}\tilde{\mathbf{v}}_{\mathrm{b}} & \tilde{\mathbf{y}}_{\mathrm{b}}(\tilde{\tilde{\mathbf{l}}}_{\mathrm{b}} - \tilde{\mathbf{l}}_{0_{\mathrm{b}}}) - \tilde{\mathbf{l}}_{0_{\mathrm{b}}}\tilde{\boldsymbol{\sigma}}_{\mathrm{b}} & \tilde{\mathbf{v}}_{\mathrm{b}}\tilde{\mathbf{y}}_{\mathrm{b}}\tilde{\tilde{\mathbf{l}}}_{\mathrm{b}}^{-1}\tilde{\tilde{\mathbf{g}}}_{\mathrm{b}}^{\mathrm{T}}\mathbf{B}^{\mathrm{T}} \\
-\tilde{\mathbf{v}}_{\mathrm{b}}\tilde{\mathbf{l}}_{0_{\mathrm{b}}}^{2}\tilde{\mathbf{l}}_{\mathrm{b}}^{-1}\tilde{\mathbf{g}}_{\mathrm{b}}^{\mathrm{T}}\mathbf{B}^{\mathrm{T}} & (3\tilde{\mathbf{l}}_{0_{\mathrm{b}}}^{2} - 2\tilde{\mathbf{l}}_{0_{\mathrm{b}}}\tilde{\mathbf{l}}_{\mathrm{b}})\tilde{\mathbf{v}}_{\mathrm{b}} & -\tilde{\mathbf{l}}_{0_{\mathrm{b}}}^{2}(\tilde{\mathbf{l}}_{\mathrm{b}} - \tilde{\mathbf{l}}_{0_{\mathrm{b}}}) - \frac{\pi}{2}\tilde{\mathbf{v}}_{\mathrm{b}} & 0 \\
-\tilde{\mathbf{v}}_{\mathrm{b}}\tilde{\mathbf{l}}_{0_{\mathrm{b}}}^{2}\tilde{\tilde{\mathbf{l}}}_{\mathrm{b}}^{-1}\tilde{\tilde{\mathbf{g}}}_{\mathrm{b}}^{\mathrm{T}}\mathbf{B}^{\mathrm{T}} & (3\tilde{\mathbf{l}}_{0_{\mathrm{b}}}^{2} - 2\tilde{\mathbf{l}}_{0_{\mathrm{b}}}\tilde{\tilde{\mathbf{l}}}_{\mathrm{b}})\tilde{\mathbf{v}}_{\mathrm{b}} & -\tilde{\mathbf{l}}_{0_{\mathrm{b}}}^{2}(\tilde{\tilde{\mathbf{l}}}_{\mathrm{b}} - \tilde{\mathbf{l}}_{0_{\mathrm{b}}}) - \frac{\pi}{2}\tilde{\mathbf{v}}_{\mathrm{b}} & -\tilde{\mathbf{v}}_{\mathrm{b}}\tilde{\mathbf{l}}_{0_{\mathrm{b}}}^{2}\tilde{\tilde{\mathbf{l}}}_{\mathrm{b}}^{-1}\tilde{\tilde{\mathbf{g}}}_{\mathrm{b}}^{\mathrm{T}}\mathbf{B}^{\mathrm{T}}
\end{bmatrix}.$$

3.2. Solution method

The solutions for the example problems given in the following section are obtained using the SNOPT 6.1 software package for sparse nonlinearly constrained optimization (see Gill et al., 1997, 2005). The package uses the sequential quadratic programming (SQP) method. All constraint Jacobians and objective gradients were made available during the execution of the code in its sparse mode. The SNOPT package has several features that are exploited in the optimization of tensegrity structures.

- The package exploits general sparsity in the constraint Jacobian matrix (see Fig. 1).
- As the iterations proceed, SNOPT builds a quasi-Newton approximation to the second-derivatives of the Lagrangian function. No second derivatives need be provided by the user.
- SNOPT computes a feasible point for the linear constraints and simple bound constraints before evaluating the nonlinear constraint functions. Once the linear constraints are feasible, they are never allowed to go infeasible.
- If the nonlinear constraints are infeasible, SNOPT will find a point that locally minimizes the one-norm of the nonlinear constraint violations.

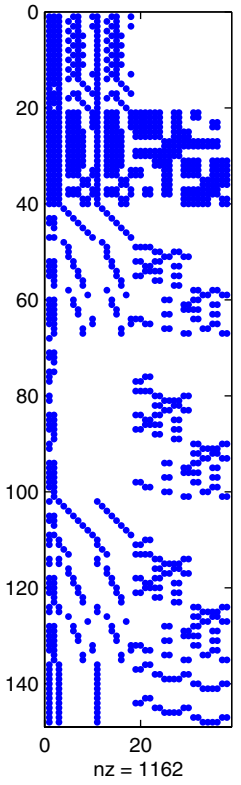

Fig. 1. Typical sparsity pattern of the Jacobian of the nonlinear constraints excluding general shape constraint for symmetric problem.

Numerical optimization methods have already been applied to large deformation static analysis of structures. Unlike the unconstrained energy minimization method used by Coyette and Guisset (1988) for analysis of large deformations of cable networks, our approach uses an explicit formulation of equilibrium conditions of unloaded and loaded prestressed structures. These equilibrium conditions actually characterize stationary points of the energy functional in the aforementioned work.

4. Examples

4.1. Asymmetric planar cantilevered tensegrity beam under bending load

The tensegrity structure in Fig. 2 illustrates the result of applying the optimization algorithm to the 2D tensegrity cantilevered beam. This tensegrity beam is constructed from three planar tensegrity crosses, with an aspect ratio of seven. The structure is attached to the fixed supports at the two leftmost nodes. The structure is loaded with a unit vertical force acting at the top right node. In the initial symmetric configuration the structure satisfies all the design constraints.

Depending on the initial guess for the variables in the problem the optimization algorithm found different optimal solutions with the same value of the objective function (see Fig. 3). The optimized structure in Fig. 3 has very similar geometry $\mathbf{p}$ as the optimized structure in Fig. 2, but significantly different distribution of the variables $\mathbf{l}_0$, and $\mathbf{v}$. For example, the total rest length of the elements are significantly different in these

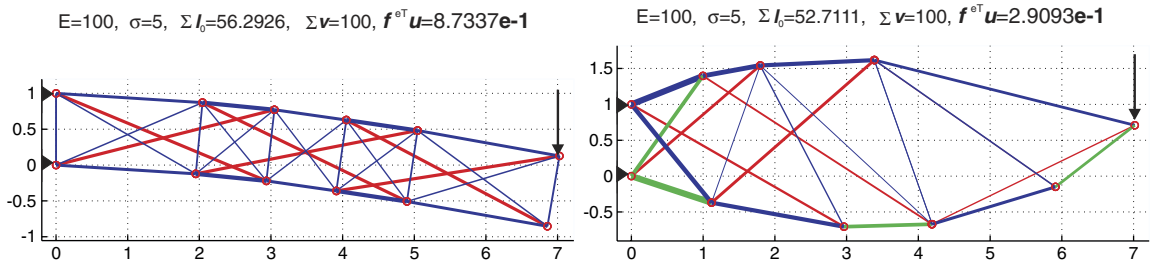

Fig. 2. Initial vs. optimized tensegrity beam design in loaded state, showing deformation under load. *Legend*: green (light gray)—slack strings, red (dark gray)—compressed bars, black (blue)—stretched strings. (For interpretation of the references in colour in this figure legend, the reader is referred to the web version of this article.)

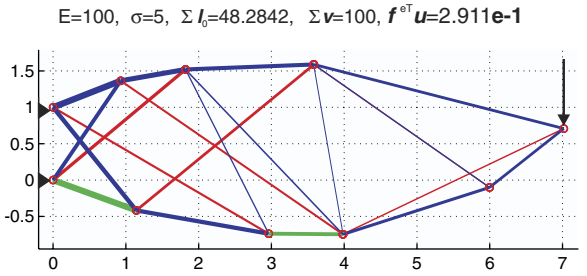

Fig. 3. Non-uniqueness of the optimal structure—an alternative optimal structure.

two optimal structures, i.e., $\sum \mathbf{l}_0 = 52.7111$, and $\sum \mathbf{l}_0 = 48.2842$, respectively. The set of active constraints (the inequality constraints satisfied with equality) in these two optimal configuration are also different. Observe that only two strings are marginally slack in the second example, compared to four strings in the first example. The slightly different values of the objective function can be attributed to the fact that the optimization algorithm is terminated when the necessary conditions for optimality are satisfied to within a small user-specified tolerance.

From these results we conclude that:

- optimal topologies are highly asymmetric;
- there exist more than one optimal structure;
- class-two tensegrity topologies where some bars touch each other are advantageous.

4.2. Symmetric planar cantilevered tensegrity beam under bending load

In the example of Fig. 4 additional symmetry constraints are imposed. The initial and optimized structure are depicted in the undeformed configurations. The nodal position vector, $\mathbf{p}$, and the distribution of the parameters $\mathbf{l}_0$, and $\mathbf{v}$, admit symmetry with respect to the horizontal axis of the structures. The structure is attached to the fixed supports at the two leftmost nodes. The unit vertical force is applied at the top right node. The length, L, of the structure is fixed, so that the y-coordinate, of the nodes at the end of the beam, defined by d is a free variable. Observe that an equivalent formulation of the yield strength constraint may be obtained by dividing it by the yield stress σ. Hence, this material parameter is substituted in the problem with the material yield strain, σ/y, that modifies the direction of the constraint Jacobian. Increasing the

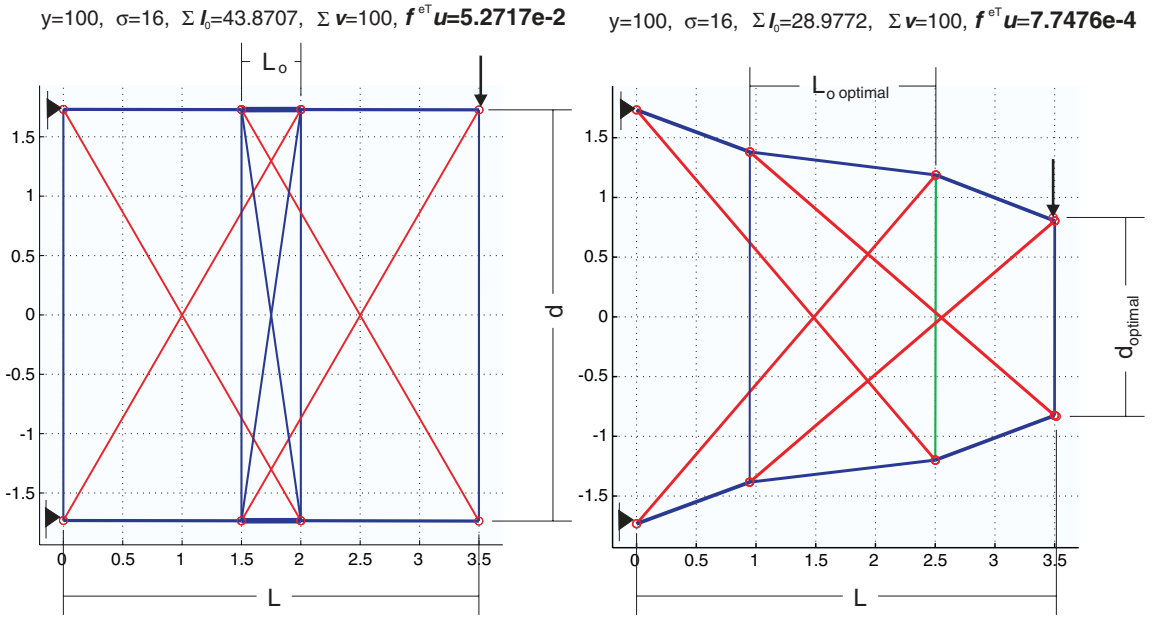

Fig. 4. Initial vs. optimal aspect ratio L/d of symmetric tensegrity beam.

value of the material σ/y ratio, effectively makes the yield stress constraint less restrictive with respect to other constraints. Larger values of the yield strain correspond to rubber-like materials that can undergo large elastic deformation, whereas the small yield strain pertains to the more traditional, metal-like, engineering materials.

The material Young's module y and the yield strain σ/y are varied to investigate their impact on the parameters that characterize overall shape of the optimal design of the two stage tensegrity beam. These shape parameters are defined in Fig. 4. The results shown in Fig. 5 lead to the following conclusions:

- Overlap ratio, L_0/L, between stages exhibits a significant sensitivity to the variation of both y, and σ/y in the neighborhood of $\sigma/y = 0.1$. Outside this region, it monotonically increases with the increase of the yield strain, σ/y, and is not sensitive to the variations of y.
- The truncation ratio, d/L, of the structure monotonically decreases with the increase of the yield strain, σ/y, and is not sensitive to the variations of y.

The increase of the overlap ratio between stages, with the increase of the yield strain, is consistent with the analytical result of Jager and Skelton (2001), which shows that the stiffness of the planar tensegrity beam, without any additional constraints, is optimized when stages completely overlap, i.e., when $L_0/L = 1$. Note that increasing the yield strain σ/y makes the feasible domain larger, and the analysis becomes similar to the unconstrained stiffness analysis in the work of Jager and Skelton (2001).

4.3. Symmetric tensegrity tower under compressive load

The symmetric tensegrity tower design in Fig. 6 is obtained by optimizing the geometry of the modified two stage shell-class tensegrity structure. This structure with the connectivity defined by Skelton et al. (2001), is modified by including the additional strings in the connectivity scheme. A symmetric compressive

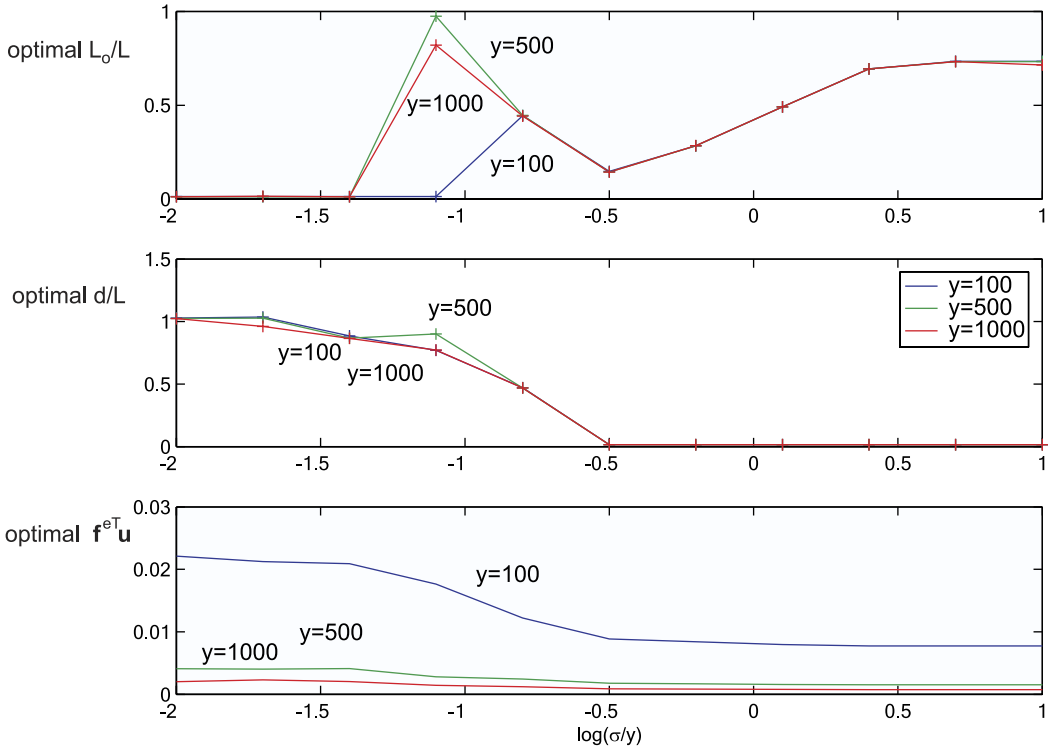

Fig. 5. Optimal overlap ratio L_0/L, truncation ratio d/L, and objective function $\mathbf{f}^{T}\mathbf{u}$ vs. material yield strain σ/y.

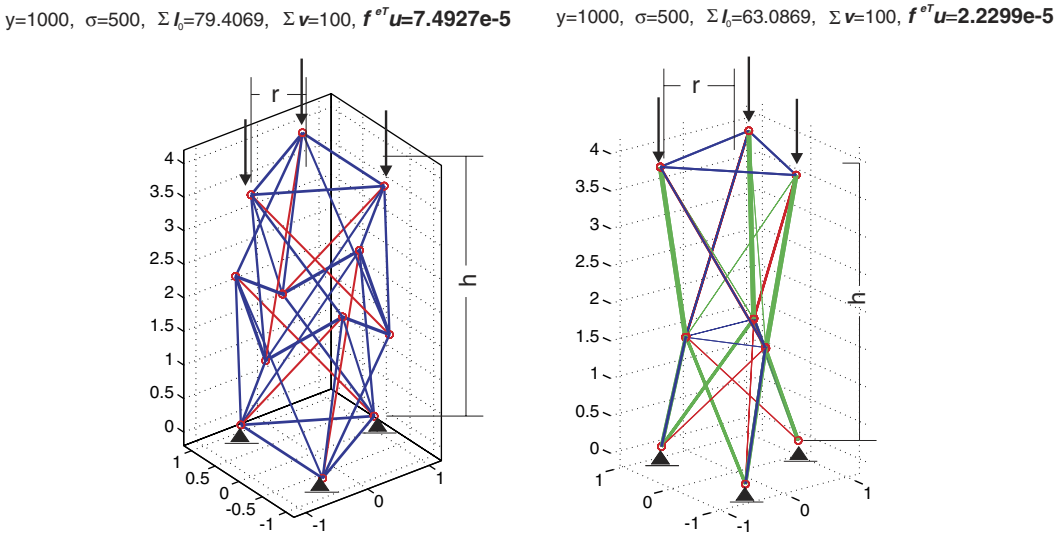

Fig. 6. Initial vs. optimal tensegrity tower under compressive load.

load is applied at the top nodes of the structure. The bottom nodes of the structure are attached to the fixed supports. From this example, we may infer the following:

- Class-two tensegrity towers for which the bars of the adjacent stages are connected at a node are superior in stiffness to class-one structures for which the bars do not touch.

This result is to be expected since the path of the load transmission from the top of the structure to the supports is shorter in this case.

4.4. Optimal number of stages

In this section, the optimal number of stages of a planar tensegrity beam is investigated. As in the two previous planar examples, the tensegrity beam is supported at the two leftmost nodes and loaded with the unit vertical force acting at the top-right node. The shape of the structure is constrained to admit the symmetry with respect to the horizontal axis. Tapering of the stages is not allowed. All stages have the same

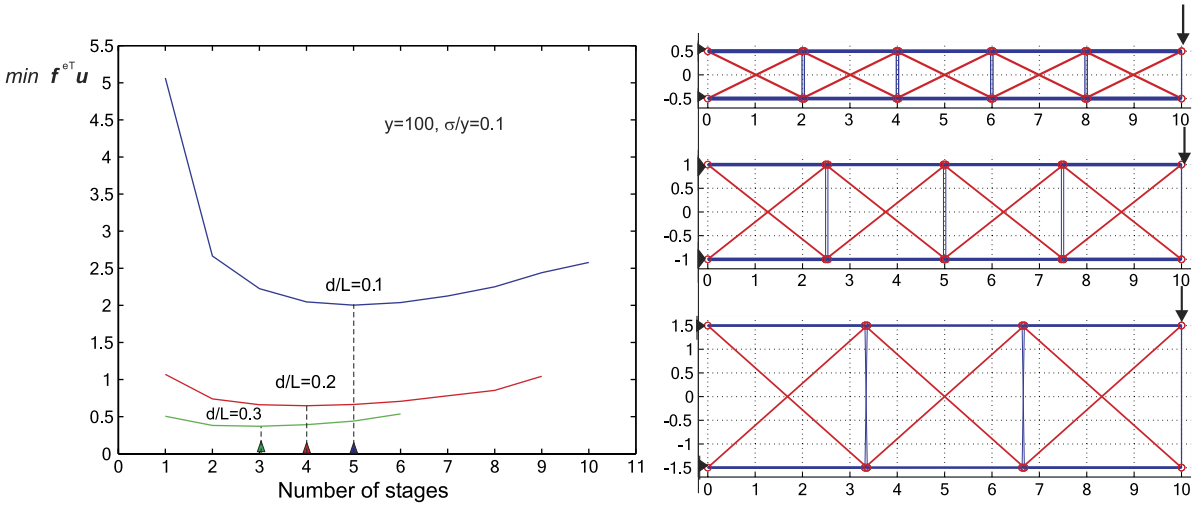

Fig. 7. Optimal number of stages vs. tensegrity beam aspect ratio.

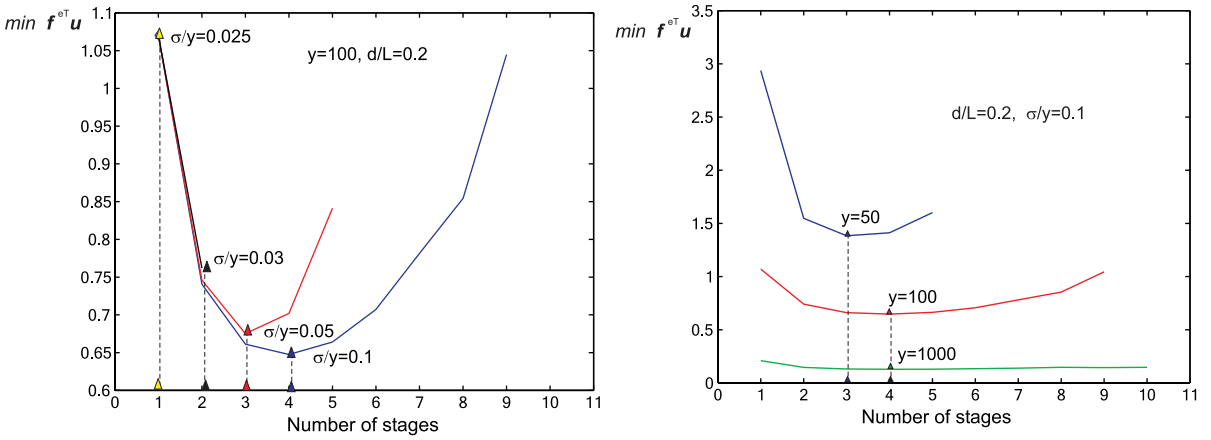

Fig. 8. Optimal number of stages of tensegrity beam vs. material parameters.

shape, and their positions in the structure can be characterized by the one-dimensional lattice formed of the centers of the stages, as indicated in Fig. 7. The families of curves depicted in Figs. 7 and 8 are generated by running a sequence of optimization problems, in which the number of stages of the tensegrity beam varies between one and the first value at which a loss of constraint feasibility occurs.

From these results the following may be inferred:

- For a fixed material, the optimal number of stages decreases as the beam aspect ratio, d/L, increases, and the sensitivity is large for the larger ratio d/L.
- For a fixed beam aspect ratio d/L, and Young's module y, the optimal number of stages increases as the material yield strain σ/y increases, but the sensitivity to the yield strain variation decreases.
- For a fixed beam aspect ratio and a fixed material yield strain σ/y, the optimal number of stages increases as the Young's module y increases, and the sensitivity to this variation decreases.

5. Discussion

Our results show that class-one tensegrity structures with a discontinuous network of compressive elements are more favorable for materials with a high yield strain. This may explain why these configurations occur in some biological structures, and the success of class-one tensegrities in modeling cytoskeleton (see, e.g., Coughlin and Stamenović, 1997; Wang et al., 2001). The benefit of utilizing class-one structures is twofold. Not only can they undergo larger shape changes as shown in Masic and Skelton (2002), but as we have shown here, this can be accomplished at no stiffness penalty for certain materials. This is a clear advantage for biological systems that predominantly utilize materials with high yield strains.

By inspecting the stiffness matrix of prestressed structures given by Masic et al. (2005) and Masic and Skelton (in press), it can be shown that increasing prestress in a structure affects its stiffness. Moreover, the sensitivity of the stiffness matrix condition number to this change increases as the material yield strain increases. This leads to the conclusion that a significant stiffening of a structure because of the prestress may be expected only in structures of materials with relatively high yield strains. Most biological materials belong to this category, which may explain a noticeable sensitivity of the cytoskeleton stiffness to prestress change, as several researchers have verified, e.g., Stamenovic et al. (1996).

In class-one tensegrity structures with the minimum feasible number of elements, there usually exist soft eigenmodes of the stiffness matrix. If these structures are not significantly prestressed, their stiffness matrix has a very high condition number. There are three ways to stiffen these soft modes:

- increase the prestress;
- add extra elements to remove the soft modes; or
- change to a class-two structure.

We investigate these three options for structures of different material yield strains.

For a low material yield strain, increasing the prestress has the effect of moving small eigenvalues of the symmetric stiffness matrix away from zero, but the magnitude of the increase relative to the eigenvalues of the high stiffness modes is negligible. This is because the large eigenvalues of the stiffness matrix are proportional to Young's modulus y, whereas the eigenvalues associated with the soft modes are proportional to the prestress σ. This prestress at its highest allowed value (yield stress) is still very small compared to Young's modulus. Adding extra elements to the structures requires allocating extra material to build them. Hence, the third option of using a class-two structure seems most favorable for structures of a low material yield strain.

In structures with materials that have high yield strain, the significant contribution of the prestress explains why class-two structures are not inferior to class-one structures. By using a smaller number of elements to allow more material to be allocated for remaining elements, in conjunction with a significantly increased prestress, it is possible to obtain an efficient structure with a well-conditioned stiffness matrix.

As is well known, some geometric configurations yield superior stiffness properties. Our results indicate that there also exist configurations that lead to a larger impact of the prestress, which in some materials predominantly contributes to the structure stiffness. Our results identify those configurations for the tensegrity beam.

6. Conclusions

Tensegrity structures have been around for fifty years, without the necessary analytical tools to make the tensegrity paradigm an effective engineering alternative. This paper takes a large step toward improving this situation, by providing an optimization methodology. Unlike methods that only find feasible tensegrity geometries, this paper proposes a systematic procedure for designing optimal tensegrity structures. An important contribution of this paper toward deriving more advanced tensegrity design tools, was the inclusion of yield and buckling constraints of structural members. The choice for the design variables and the way that the constraints are formulated clearly display their interconnections and suggests efficient ways of scaling the constraints to improve efficiency of the numerical optimization algorithms.

One of the novelties introduced in this paper is the utilization of optimization methods for solving nonlinear static response problems associated with large nodal displacements. In addition to a higher accuracy in predicting a static response of a structure, this method enables efficient solutions of the problems in structures that have ill-conditioned or even singular stiffness matrices at no additional cost. It also indirectly incorporates global buckling as a possible mode of the deformation of the structure.

There is no guarantee that the results shown here represent global optimal solutions because of the nonconvex nature of the optimization problem. In some instances, repeated solutions increased our confidence to draw several general conclusions. This paper demonstrates that,

- optimization of tensegrity topology and geometry, cast in the form of the nonlinear program, is effectively solvable; and
- if the problem is feasible, the optimization approach is an appropriate design tool that guarantees a monotonic stiffness improvement compared to the initial design.

References

Bendsoe, M.P., 1995. Optimization of Structural Topology, Shape, and Material. Springer.

Bendsoe, M.P., Kikuchi, N., 1988. Generating optimal topologies in structural design using a homogenization method. Computer Methods in Applied Mechanics and Engineering 71 (2), 197–224.

Ben-Tal, A., Nemirovski, A., 1997. Robust truss topology design via semidefinite programming. SIAM Journal of Optimization 7 (4), 991–1016.

Ben-Tal, A., Kočvara, M., Nemirovski, A., Zowe, J., 1999. Free material design via semidefinite programming: the multiload case with contact conditions. SIAM Journal of Optimization 9 (4), 813–832.

Connelly, R., Terrell, M., 1995. Globally rigid symmetric tensegrities. Structural Topology 21, 59–78.

Connelly, R., Whiteley, W., 1996. Second order rigidity and prestress stability for tensegrity frameworks. SIAM Journal of Discrete Mathematics 9 (3), 453–491.

Coughlin, M.F., Stamenović, D., 1997. A tensegrity structure with buckling compression elements: application to cell mechanics. Transactions of ASME—Journal of Applied Mechanics 64, 480–486.

Coyette, J., Guisset, P., 1988. Cable network analysis by a nonlinear programming technique. Engineering Structures 10 (1), 41–46.
de Jager, B., Skelton, R., 2001. Optimizing stiffness properties of tensegrity structures. In: Proceedings of International Mechanical Engineering Congress and Exposition 2001, New York.
Diaz, A.R., Bendsoe, M.P., 1992. Shape optimization of structures for multiple loading conditions using a homogenization method. Structural Optimization 4 (1), 17–22.
Gill, P.E., Murray, W., Saunders, M.A., 1997. User's guide for SNOPT 5.3: a Fortran package for large-scale nonlinear programming. Numerical Analysis Report 97-5. Department of Mathematics, University of California, San Diego, La Jolla, CA.
Gill, P.E., Murray, W., Saunders, M.A., 2005. SNOPT: an SQP algorithm for large-scale constrained optimization. SIAM Review 47, 99–131.
Hanaor, A., 1991. Double-layer tensegrity grids—static load response. 1. Analytical study. Journal of Structural Engineering—ASCE 117 (6), 1660–1674.
Jarre, F., Kocvara, M., Zowe, J., 1998. Optimal truss design by interior-point methods. SIAM Journal of Optimization 8 (4), 1084–1107.
Kanchanasaratool, N., Williamson, D., 2002. Modeling and control of class nsp tensegrity structures. International Journal of Control 75 (2), 123–139.
Masic, M., Skelton, R.E., 2002. Deployable plates made from stable-element class 1 tensegrity. In: Proceedings of the 9th Smart Structures and Materials Conference. International Society for Optical Engineering (SPIE), Belligham, WA, USA, pp. 220–230.
Masic, M., Skelton, R.E., 2005. Path planning and open-loop shape control of modular tensegrity structures. AIAA Journal of Guidance, Control, and Dynamics 28 (3), 421–430.
Masic, M., Skelton, R.E., Gill, P.E., 2005. Algebraic tensegrity form-finding. International Journal of Solids and Structures 42 (16–17), 4833–4858, doi: 10.1016/j.ijsolstr.2005.01.014.
Masic, M., Skelton, R.E., in press. Selection of prestress for optimal dynamic/control performance of tensegrity structures. International Journal of Solids and Structures, doi:10.1016/j.ijsolstr.2005.06.066.
Motro, R., 1992. Tensegrity systems: the state of the art. International Journal of Space Structures 7 (2), 75–83.
Murakami, H., 2001. Static and dynamic analysis of tensegrity structures. Part 1: nonlinear equations of motion. International Journal of Solids and Structures 38 (20), 3599–3613.
Pellegrino, S., 1992. A class of tensegrity domes. International Journal of Space Structures 7 (2), 127–142.
Rozvany, G.I.N., Prager, W., 1989. Structural Design via Optimality Criteria: The Prager Approach to Structural Optimization. Kluwer Academic Publishers, Dordrecht.
Save, M., Prager, W., Sacchi, G., 1985. Structural Optimization, Optimality Criteria, Mathematical Concepts and Methods in Science and Engineering. Kluwer Academic Publishers.
Skelton, R., Adhikari, R., 1998. An introduction to smart tensegrity structures. In: Proceedings of the 12th ASCE Engineering Mechanics Conference.
Skelton, R.E., Pinaud, J., Mingori, D.L., 2001. Dynamics of the shell-class of tensegrity structures. Journal of the Franklin Institute 2–3 (338), 255–320.
Stamenovic, D., Fredberg, J., Wang, N., Butler, J., Ingber, D., 1996. A microstructural approach to cytoskeletal mechanics based on tensegrity. Journal of Theoretical Biology 181 (2), 125–136.
Sultan, C., Corless, M., Skelton, R., 2000. Tensegrity flight simulator. Journal of Guidance, Control, and Dynamics 23 (6), 1055–1064.
Sultan, C., Corless, M., Skelton, R.E., 2002. Symmetric reconfiguration of tensegrity structures. International Journal of Solids and Structures 39 (8), 2215–2234.
Vasart, N., Motro, R., 1999. Multiparametered formfinding method: application to tensegrity systems. International Journal of Space Structures 14 (2), 147–154.
Wang, N., Naruse, K., Stamenovic, D., Freedberg, J., Mijailovic, S., Toric-Norrelykke, I., Polte, T., Manix, R., Ingber, D., 2001. Mechanical behavior in living cells consistent with the tensegrity model. Proceedings of the National Academy of Sciences of the United States of America, 7765–7770.